

## ORIGINAL ARTICLE

Paola Rossi · Egidio D'Angelo · Jacopo Magistretti  
Mauro Toselli · Vanni Taglietti

## Age-dependent expression of high-voltage activated calcium currents during cerebellar granule cell development in situ

Received: 27 December 1993 / Received after revision: 28 March 1994 / Accepted: 17 May 1994

**Abstract**  $\text{Ca}^{2+}$  currents play a crucial role during neuronal growth. In this paper we describe the development of  $\text{Ca}^{2+}$  currents using whole-cell patch-clamp recordings in granule cells of cerebellar slices obtained from 7- to 24-day-old rats. Granule cells expressed high-voltage-activated (HVA)  $\text{Ca}^{2+}$  currents in different proportions. The percentage of cells with a measurable HVA current, and the size of HVA current increased in parallel with granule cell maturation. At less than 14 days HVA currents consisted of a fast- and slow-inactivating component, while at more than 19 days only the slow-inactivating component remained. The fast-inactivating component had faster activation and inactivation kinetics, a more negative threshold for activation, and steeper steady-state inactivation than the slow-inactivating component. Nifedipine (5  $\mu\text{M}$ ) partially blocked both components.  $\omega$ -Conotoxin (5  $\mu\text{M}$ ,  $\omega$ -CgTx) blocked the slow-inactivating component rather selectively. These results indicate that HVA currents change their gating and pharmacological properties during development. Although the mechanism at the molecular level remains speculative, the developmental changes of the HVA current are relevant to the processes of granule cell maturation and excitability.

**Key words** Calcium channels · Calcium currents  
Cerebellum · Development · Neuron · Patch-clamp

### Introduction

Different types of voltage-activated channels regulate  $\text{Ca}^{2+}$  inflow through the neuronal membrane. Depending on the threshold for activation, neuronal  $\text{Ca}^{2+}$  channels can be classified as high-voltage activated (HVA) and low-voltage activated (LVA). HVA and LVA channels

differ also as to their pharmacological sensitivity and kinetics [8]. HVA channels can be further distinguished as L-, N-, and P-type according to their pharmacological properties (for recent reviews see [24, 35]).

It is widely accepted that  $\text{Ca}^{2+}$  inflow through the plasma membrane plays a major role in controlling neuronal excitability, neurotransmitter release, and neurogenesis [2]. So far, development of neuronal  $\text{Ca}^{2+}$  currents has been studied mostly in cell culture [4, 39], and in acutely isolated neurons [36]. In this study, we used cerebellar slices obtained from rats of different ages and recorded  $\text{Ca}^{2+}$  currents from granule cell neurons in the whole-cell patch-clamp configuration [15]. Recent experimental and modelling work has shown that cerebellar granule cells are electrotonically quite compact [38], and that no relevant electronic changes occur during the 2nd and 3rd postnatal week [12]. Therefore this method, in addition to showing  $\text{Ca}^{2+}$  currents in the native tissue, should allow establishment of  $\text{Ca}^{2+}$  current expression at a specific developmental stage [13].

The rat cerebellar granule cell has been intensely investigated as a model of neuronal development in the central nervous system [7]. Cerebellar granule cell maturation occurs after birth following a regular timetable consisting of migration in the internal granular layer, formation of synaptic contacts, and development of mature morphological and functional properties [1, 20, 30]. The major morphological and functional changes have been reported to terminate by the end of the 3rd postnatal week.

$\text{Ca}^{2+}$  inflow in granule cells is provided through different pathways, including *N*-methyl-D-aspartate- (NMDA)-receptor-activated ion channels and voltage-activated  $\text{Ca}^{2+}$  channels.  $\text{Ca}^{2+}$  inflow is required for granule cell survival, neurite outgrowth, and migration [7, 23, 24]. Studies in which cerebellar granule cells in culture were used reported the presence of HVA currents either of the L-type [25], or with both L and N pharmacological properties [14, 21]. Recently, an N-like current with unusually fast kinetics has been described [16]. Kinetic investigation of whole-cell currents revealed the existence of

P. Rossi · E. D'Angelo (✉) · J. Magistretti · M. Toselli  
V. Taglietti  
Institute of General Physiology, Via Forlanini 6,  
I-27100 Pavia, Italy

two components [31], the origins of which remain controversial. In fact, single-channel recordings suggested either that just one  $\text{Ca}^{2+}$  channel with complex gating properties was present [32], or that more  $\text{Ca}^{2+}$  channels were expressed in cerebellar granule cells in culture [6, 17].

We found that HVA currents *in situ* changed their amplitude, kinetics, gating, and pharmacology during development. Our results suggest that different ensemble currents observed at different ages can be explained by the coexistence of a fast- and a slow-inactivating component in different proportions.

## Materials and methods

**Slice preparation.** Cerebellar slices were obtained from 7- to 24-day-old Wistar rats (day of birth=P1) as described previously [11, 12]. Slices were cut in the parasagittal plane and were 200–300  $\mu\text{m}$  thick.

**Patch-clamp recording.** Whole-cell patch-clamp recordings were performed as reported previously [12, 15]. Patch pipettes were pulled from thick-walled borosilicate glass capillaries, and had 7–9  $\text{M}\Omega$  resistance before seal formation. Except in five neurons, the current transient induced from the holding potential of  $-80$  mV by 10-mV hyperpolarizing pulses (sampling frequency=50 kHz) had a fast mono-exponential decay. Analysis of the transient showed that these neurons had the high input resistance ( $R_m=1\text{--}5$   $\text{G}\Omega$ ), low membrane capacitance ( $C_m=2\text{--}4$  pF), and fast voltage-clamp time constant ( $\tau_{vc}=80\text{--}120$   $\mu\text{s}$ ) typical of granule cells [12, 38]. Series resistance ( $R_s$ ) was 20–30  $\text{M}\Omega$ . The same properties were found both using the blind-seal approach and recording from granule cells identified with Nomarsky optics.  $\text{Ca}^{2+}$  currents were isolated by blocking  $\text{Na}^+$  and  $\text{K}^+$  currents, and by replacing intracellular  $\text{K}^+$  by  $\text{Cs}^+$  (see solutions below). Currents were recorded at room temperature ( $19\text{--}21^\circ\text{C}$ ) using an Axopatch-1D (Axon Instruments) patch-clamp amplifier at the output cut-off frequency of 5 kHz. Currents were simultaneously stored on a DAT recorder (Biologic DTR-1201), and fed to the mass memory of a PC (sampling intervals 400–1000  $\mu\text{s}$ ).

**Data analysis.** Acquisition and data analysis were done using P-Clamp and Dempster software (J. Dempster, Department of Physiology, University of Strathclyde, Glasgow, Scotland). Leakage current was commonly subtracted using hyperpolarizing pulses delivered before the test pulse, and in some cells also by subtracting the residual current recorded after perfusion of 500  $\mu\text{M}$   $\text{CdCl}_2$ .

Data are reported as mean $\pm$ SEM, and the number of observation is indicated in brackets.

**Error estimation.** Cerebellar granule cells are composed of a small spherical soma protruding four tiny dendrites and an axon, the ascending branch of parallel fibres [20]. The axon is thin (diameter of 0.1  $\mu\text{m}$ ) and contributes less than 15% to the total input conductance (unpublished). Since cerebellar granule cells had a high  $R_m/R_s$  ratio (about 200 times), the voltage-clamp error introduced by  $R_s$  was negligible (0.5 mV/100 mV, see also [12]).

At a first approximation cerebellar granule cells can be treated as a single electrical compartment [12, 33]. This approximation was used to calculate the cut-off frequency response of the whole electrode plus cell system in voltage-clamp conditions,  $f_{vc}$ . The decay of passive current transients was fitted by a single exponential function with a time constant,  $\tau_{vc} = R_s C_m$  (see above), and an  $f_{vc}$  value of  $1/2 \pi \tau_{vc}$  ( $-3$  dB attenuation) was calculated. With an average  $\tau_{vc}$  value of 110  $\mu\text{s}$ ,  $f_{vc}$  was 1.5 kHz (range 1.2–2 kHz). Conductance changes occurring at a frequency less than 1.5 kHz, therefore, should be substantially unaffected by voltage-clamp errors.

Finer modelling using a spherical cell body attached to an equivalent cylinder can be used to estimate the space-clamp error introduced by electrotonic distortion in the processes. The voltage attenuation of a sine wave of known frequency ( $f_c$ ) was calculated using the analytical solution of the cable equation recently used by Spruston et al. ([33], Eqs. 8–12, which are not repeated here). Voltage attenuation at the end of the equivalent cylinder was simulated using a sinusoidal potential variation in the soma with  $f_c=f_{vc}=1.5$  kHz. At the peak of  $\text{Ca}^{2+}$  currents,  $R_m$  and  $\tau_m (=R_m C_m)$  were 6-times smaller than at rest. The six-fold smaller  $R_m$  caused a 2.4-times decrease of the membrane space constant,  $\lambda$ , which made the electrotonic length  $L=1/\lambda$  to increase from its resting value of 0.04 [12, 38] to 0.096. With these parameters ( $L=0.096$ ,  $\tau_m=1$  ms,  $f_c=1.5$  kHz), the calculated attenuation was 0.977. The maximum space-clamp error was therefore of 2.3% during the fastest transitions (rising phase, tail current) of  $\text{Ca}^{2+}$  currents. At the low frequencies typical of  $\text{Ca}^{2+}$  current decay ( $<10$  Hz), however, calculated attenuation was negligible approaching the steady-state value of less than 1% reported previously [12].

**Solutions.** Krebs solution for slice cutting and recovery contained (mM): NaCl 120, KCl 2,  $\text{MgSO}_4 \cdot 7\text{H}_2\text{O}$  1.2,  $\text{NaHCO}_3$  26,  $\text{KH}_2\text{PO}_4$  1.2,  $\text{CaCl}_2$  2, glucose 11. This solution was equilibrated with 95%  $\text{O}_2$  and 5%  $\text{CO}_2$  (pH 7.4).

The extracellular recording solution contained (mM): NaCl 100,  $\text{MgCl}_2$  2, tetraethylammonium (TEA) 15,  $\text{NaHCO}_3$  26,  $\text{CaCl}_2$  5, glucose 10, 4-aminopyridine (4-AP) 4, and tetrodotoxin (TTX) 3  $\mu\text{M}$ . This solution was equilibrated with 95%  $\text{O}_2$ , 5%  $\text{CO}_2$  (pH 7.4).

The intracellular solution contained (mM): CsCl 120, TEA-Cl 20, ethyleneglycolbis-(aminoethylether)tetra-acetic acid (EGTA) 10,  $\text{MgCl}_2$  2, 4-(2-hydroxyethyl)-1-piperazinethanesulphonic acid (HEPES) 10, 4-adenosine 5'-triphosphate (Mg-ATP) 2, and adenosine 3',5'-cyclic monophosphate (cAMP) 1. The pH was adjusted to 7.2 with CsOH. With cAMP and ATP in the intracellular solution, HVA currents were recorded without appreciable run-down (5 $\pm$ 2% in the first 6 min of recording,  $n=6$ ).

The synthetic peptide  $\omega$ -conotoxin GVIA ( $\omega$ -CgTx), was obtained from Peninsula Laboratories. Bay K 8644 was a gift from Dr. Seuter, Bayer.  $\omega$  Agatoxin IVA ( $\omega$ -AGA-IVA) was obtained from International Peptides. D-2-Amino-5-phosphonovalerate (APV) and 6-cyano-7-nitroquinoxaline-2,3-dione (CNQX) were obtained from Tocris Neuramin, and bicuculline methobromide from Sigma.

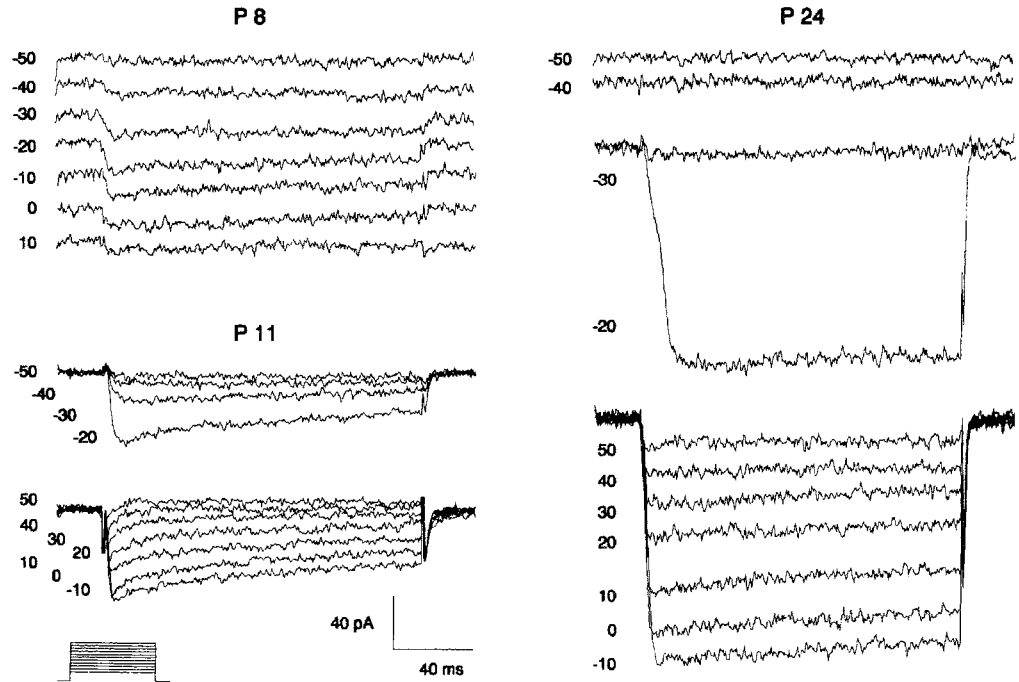
Drugs were applied locally through a multi-barrel pipette positioned 50–100  $\mu\text{m}$  away from the recorded cell.

## Results

Whole-cell patch-clamp recordings were made in 184 neurons in the inner granular layer of cerebellar slices obtained from rats aging from P7 to P24. The  $\tau_{vc}$  was  $108\pm 19$   $\mu\text{s}$  at P10–P14 ( $n=37$ ), and  $106\pm 13$   $\mu\text{s}$  at P19–P24 ( $n=25$ ). In the same cells, the whole input resistance was  $2.3\pm 0.2$   $\text{G}\Omega$  at P10–P14 ( $n=37$ ) and  $1.8\pm 0.2$   $\text{G}\Omega$  at P19–P24 ( $n=25$ ), and  $C_m$  was  $3.1\pm 0.3$  pF at P10–P14 ( $n=37$ ) and  $2.7\pm 0.4$  pF at P19–P24 ( $n=25$ ). Reported values are consistent with previous results [12, 38].

Figure 1 shows families of  $\text{Ca}^{2+}$  current recordings obtained at different ages. In all examples, currents started to activate at high potentials (between  $-40$  and  $-20$  mV) and showed slow inactivation (tens to hundreds of milliseconds) displaying, therefore, properties of HVA  $\text{Ca}^{2+}$  currents as reported also by others [14, 25, 31]. The rising phase of HVA currents was 10-times slower, and

**Fig. 1** High-voltage activated (HVA)  $\text{Ca}^{2+}$  currents in granule cells of rat cerebellar slices at different ages. HVA  $\text{Ca}^{2+}$  currents were elicited by depolarizing pulses increasing in 10-mV steps from the holding potential of  $-80$  mV. Traces are shown for 3 cells at P8, P11, and P24 (day of birth=P1). The voltage clamp protocol is indicated in the inset



the decay phase more than 500-times slower than the voltage-clamp response. Exponential fitting to the tail currents generated by current deactivation yielded time constants smaller than 1 ms at all the ages tested. We did not observe in the reported experiments abnormal kinetics (like “notchings” or slow tails) which might be interpreted as a voltage-clamp failure of the  $\text{Ca}^{2+}$  current.

#### Time course of HVA current development

Granule cell maturation was characterized by a gradual increase of the percentage of cells with appreciable HVA currents (Fig. 2A, filled circles). It should also be noted that most granule cells with HVA currents showed spontaneous synaptic activity (Fig. 2A, open circles), while cells lacking apparent  $\text{Ca}^{2+}$  currents never showed spontaneous synaptic activity. HVA current amplitude increased markedly with the age of the donor animal, as shown in Fig. 2B (top). Since granule cell  $C_m$  remained almost unchanged (Fig. 2B, bottom),  $\text{Ca}^{2+}$  current density increased proportionately to peak amplitude. Assuming a specific  $C_m$  of  $1 \mu\text{F}/\text{cm}^2$ ,  $\text{Ca}^{2+}$  current density attained values of  $0.06 \text{ mA}/\text{cm}^2$  after P20. Mean current voltage ( $I/V$ ) relationships for peak current were obtained from three groups of granule cells at P7–P8, P11–P15, and P20–P24 (Fig. 2C).  $I/V$  plots resembled closely those reported for HVA currents in granule cells and other neurons in culture.

Interestingly, we found that HVA current inactivation was more evident in immature than in mature granule cells, as indicated by the fraction of inactivated current after a 120-ms pulse normalized to peak current (Fig. 2D). The mechanism of this change was investigated by comparing the properties of HVA currents

between granule cells at two distinct stages of development, the immature stage (P10–P14) and after maturation (P19–P24).

#### Evidence for two distinct HVA current components

In immature granule cells, inactivation was fitted well by the sum of two exponentials (Fig. 3A, upper trace). The fast exponential component relaxed with a time constant of  $35 \pm 5$  ms, and was insensitive to voltage (Fig. 3B, closed circles). The slow component was 1 order of magnitude slower, and was voltage sensitive (Fig. 3B, open circles). In mature granule cells inactivation was fitted well by a single exponential (Fig. 3A, lower trace). The single inactivation component of mature cells coincided with the slower inactivation component of immature cells (Fig. 3B, squares and open circles respectively). At  $-20$  mV reliable fittings of the slow-inactivating component were obtained only in few cases. This was apparently caused by the limited duration of current traces compared to the decay time course. Exponential fitting to plots of decay time constant indicated that, at membrane potentials negative to 0 mV, the slow-inactivating component decreased by e-fold with an 8-mV depolarization, and that at potentials positive to 0 mV it remained almost constant around 300 ms.

To test whether  $\text{Ca}^{2+}$ -dependent inactivation might play a role in increasing the inactivation rate of immature currents, we replaced extracellular  $\text{Ca}^{2+}$  with  $\text{Ba}^{2+}$ , which is known to cause less HVA current inactivation than  $\text{Ca}^{2+}$  [19]. The massive spontaneous synaptic discharge which followed 5 mM  $\text{Ba}^{2+}$  perfusion usually impaired recording conditions. This unwanted effect was prevented by blocking postsynaptic receptors with  $100 \mu\text{M}$

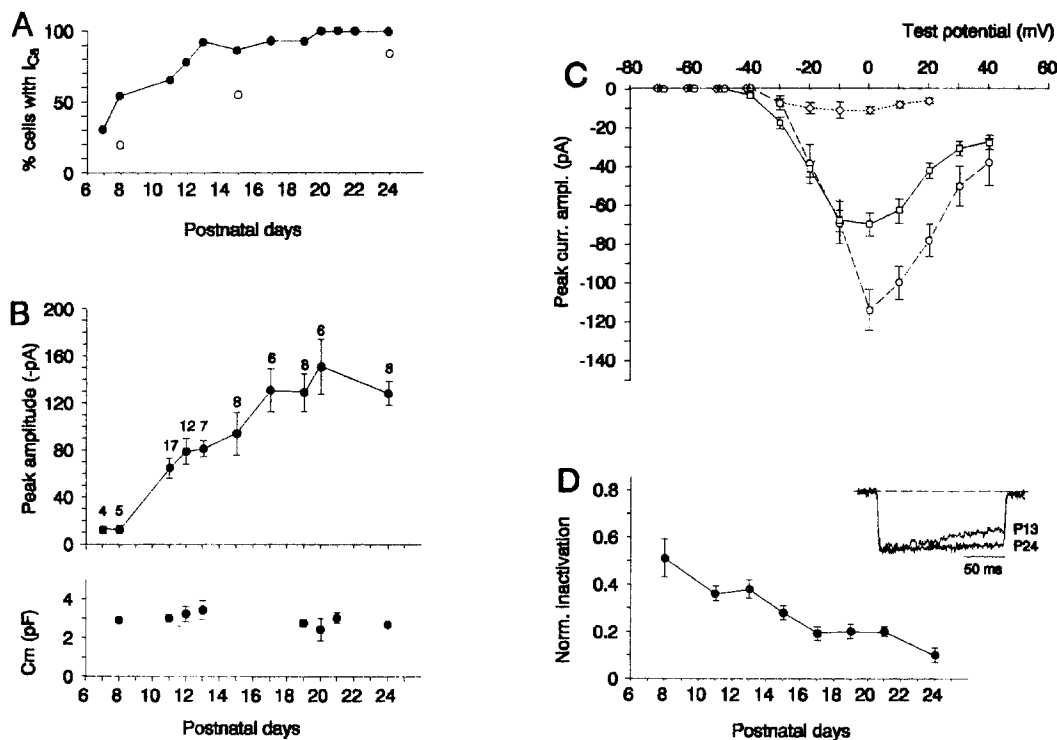


**Fig. 2A–D** Time course of HVA current development. **A** Percentage of cells with detectable HVA current. *Open circles* are the percentage of these cells which showed spontaneous synaptic activity. **B** HVA current amplitude. Value points are the mean of peak currents in different neurons (cells without appreciable  $\text{Ca}^{2+}$  currents were not included, the number of observations is indicated). The *lower plot* reports granule cell membrane capacitance ( $C_m$ ). **C** Mean current/voltage ( $I/V$ ) plots for peak HVA  $\text{Ca}^{2+}$  currents were obtained from 3 groups of cells at P7–P8 ( $n=5$ ; *diamonds*), P11–P15 ( $n=20$ ; *squares*), and P20–P24 ( $n=11$ ; *circles*). Cells without appreciable  $\text{Ca}^{2+}$  currents were not included. **D** Inactivation of HVA currents expressed as the current after a 120-ms pulse normalized to peak current. The *inset* shows two HVA currents at P13 and P24. *Error bars* indicate SEM

APV, 20  $\mu\text{M}$  CNQX, and 10  $\mu\text{M}$  bicuculline [12] (these receptor channel blockers did not change  $\text{Ca}^{2+}$  currents, not shown). In a group of six granule cells at P12, steps to 0 mV generated  $\text{Ca}^{2+}$  currents of  $-56 \pm 7$  pA, and  $\text{Ba}^{2+}$  currents of  $-52 \pm 6$  pA when measured at the peak (example tracings in inset to Fig. 3B).  $\text{Ba}^{2+}$  did not cause an obvious shift of the  $I/V$  relationships. The slight amplitude decrease with  $\text{Ba}^{2+}$  might be caused by persistence of a small amount of  $\text{Ca}^{2+}$  within the slice tissue, which is enough to severely reduce  $\text{Ba}^{2+}$  conductance [22].  $\text{Ba}^{2+}$  and  $\text{Ca}^{2+}$  currents were superimposable, excluding that increased inactivation in immature neurons was caused by  $\text{Ca}^{2+}$  influx during the test pulse. Inactivation time constants of currents where the charge carriers were either  $\text{Ca}^{2+}$  or  $\text{Ba}^{2+}$  are compared in Fig. 3B (circles and triangles, respectively).

Immature and mature HVA currents differed also as to their activation kinetics. Time to peak (ttp) decreased with membrane depolarization (Fig. 3C) and it was shorter in immature than in mature granule cells (see inset to Fig. 3C). Exponential fitting to the ttp plots yield-

ed an e-fold decrease of ttp with 42 mV and 19 mV, respectively.

#### I/V relationship and steady-state inactivation of the HVA currents

The amplitudes of the fast- and slow-inactivating current components were obtained as the amplitude of exponential curve(s) fitted to current decay. However, a reasonable estimate of the relative contribution of the two components was obtained by using the amplitude at the end of the pulse as an estimate of the slow-inactivating current component, and by measuring the amplitude of the fast-inactivating current component (in immature granule cells) as the difference between the peak amplitude and amplitude at the end of the pulse. Due to its simplicity, this method was adopted to measure the amplitude of the two current components in this section and in the section on current pharmacology (see below). It should be noted that this method, however, slightly underestimated the slow-inactivating component and slightly overestimated the fast-inactivating component, because the slow component slightly decayed with time.

The fast-inactivating component had activated already at  $-40$  mV, while the slow-inactivating component activated at  $-20$  mV (Fig. 3D). Moreover, since the fast-inactivating component peaked at the same test potential as the slow-inactivating component (0 mV), the voltage dependence of activation was less steep for the fast- than for the slow-inactivating component.

Steady-state inactivation of the HVA current was measured from  $\text{Ca}^{2+}$  currents recorded on step depolarization to 0 mV following conditioning pulses of 10 s duration between  $-100$  mV and  $-20$  mV (Fig. 4A). Inac-

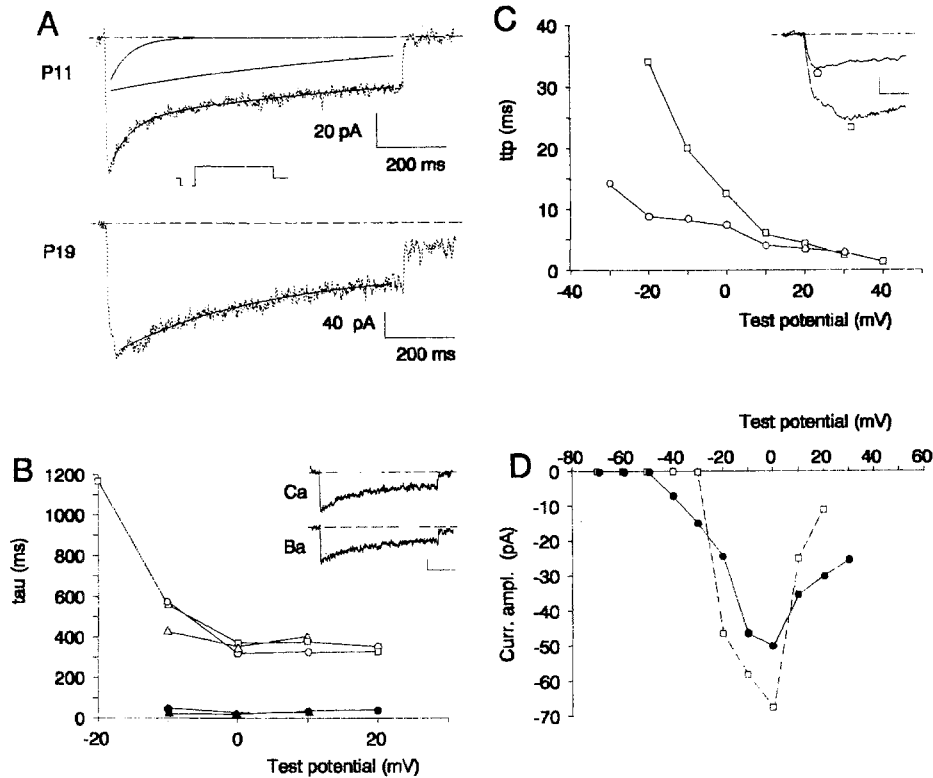


**Fig. 3A–D** Properties of the two HVA Ca<sup>2+</sup> current components. **A** Ca<sup>2+</sup> currents (dots) and fitted exponential curves (solid lines). Note that activation of Ca<sup>2+</sup> currents is from the conditioning potential of  $-100$  mV (10 s to the test potential of 0 mV, while deactivation is to the holding membrane potential of  $-60$  mV). With this voltage-clamp protocol (inset) an apparent leakage current was produced due to incomplete subtraction after termination of the test pulse. Leakage differences following deactivation were proportional to the input resistance ( $4.7$  G $\Omega$  and  $2.9$  G $\Omega$  in the upper and lower traces, respectively). Immature granule cell (P11): two exponential functions are required to fit current decay ( $\tau_1=55$  ms,  $\tau_2=588$  ms). The global function (enhanced line) is superimposed to the trace. Mature granule cell (P20): one exponential function (enhanced line) is required to fit current decay ( $\tau_1=321$  ms). **B, C, D** The voltage dependence of Ca<sup>2+</sup> currents in two groups of cells at P11–P14 (circles), and at P19–P24 (squares). **B** Inactivation time constants of HVA Ca<sup>2+</sup> currents obtained with exponential fittings in immature (circles,  $n=11$ ), and mature (squares,  $n=5$ , but  $n=3$  at  $-20$  mV) granule cells. Filled symbols indicate the fast-inactivating component (SEM $<7$  ms), open symbols indicate the slow-inactivating component (SEM $<140$  ms). Ba<sup>2+</sup> currents were also recorded from 6 of the cells at P11–P14 (triangles,  $n=6$ , but  $n=3$  at  $-20$  mV). The inset shows Ca<sup>2+</sup> and Ba<sup>2+</sup> currents in the same cell at P13 (calibration 20 pA, 200 ms). **C** Time to peak (ttp) of HVA Ca<sup>2+</sup> currents in immature (circles,  $n=5$ ; SEM $<1.4$  ms), and in mature (squares,  $n=5$ ; SEM $<1.3$  ms) granule cells. The inset illustrates an example of rising phases in immature and mature Ca<sup>2+</sup> currents (calibration 50 pA, 20 ms). **D** I/V plots for the fast-inactivating component (filled circles,  $n=11$ ; SEM $<9$  pA) and the slow-inactivating component in immature granule cells (open squares,  $n=5$ ; SEM $<14$  pA)

tivation plots for normalized peak amplitude versus holding potentials were constructed, and data points were fitted by a Boltzmann equation (Fig. 4B). Data were compared between two groups of immature and mature granule cells. Fitting curves clearly show a shift of about 15 mV towards more negative potentials of the fast-inac-

tivating current component ( $V_{1/2}=-62$  mV,  $k=11$ ) with respect to the slow-inactivating component, both in immature ( $V_{1/2}=-49$  mV,  $k=15$ ) and mature granule cells ( $V_{1/2}=-48$  mV,  $k=15$ ).

Therefore, the fast- and slow-inactivating components of HVA Ca<sup>2+</sup> current had different gating properties, and gating properties of the slow-inactivating component were similar in immature and mature preparations.

#### Pharmacology of the HVA currents

The snail venom  $\omega$ -CgTx blocks selectively the N-type HVA current (see [9]).  $\omega$ -CgTx (5  $\mu$ M) reduced the amplitude of the HVA current both in immature and mature granule cells (Fig. 5). In order to verify whether the fast- and slow-inactivating components were affected differently by the action of  $\omega$ -CgTx, we measured the amplitude of the fast- and slow-inactivating component as explained above. The slow-inactivating component (Fig. 5) was reduced by  $94\pm 9\%$  ( $n=13$ ) in mature and by  $60\pm 8\%$  ( $n=9$ ) in immature preparations. Amplitude of the fast-inactivating component was reduced by  $19\pm 5\%$  ( $n=9$ ). In fact, reduction of the fast-inactivating component was at least partially explained by the measuring technique, since the slow-inactivating component was usually greater at the peak than at the end. Indeed, subtraction of traces after application of  $\omega$ -CgTx from control traces showed that the  $\omega$ -CgTx-sensitive current had slow kinetics (Fig. 5A), indicating that the fast component was virtually unaffected. The action of  $\omega$ -CgTx was voltage insensitive and persisted following prolonged washing (up to 20 min, not shown).

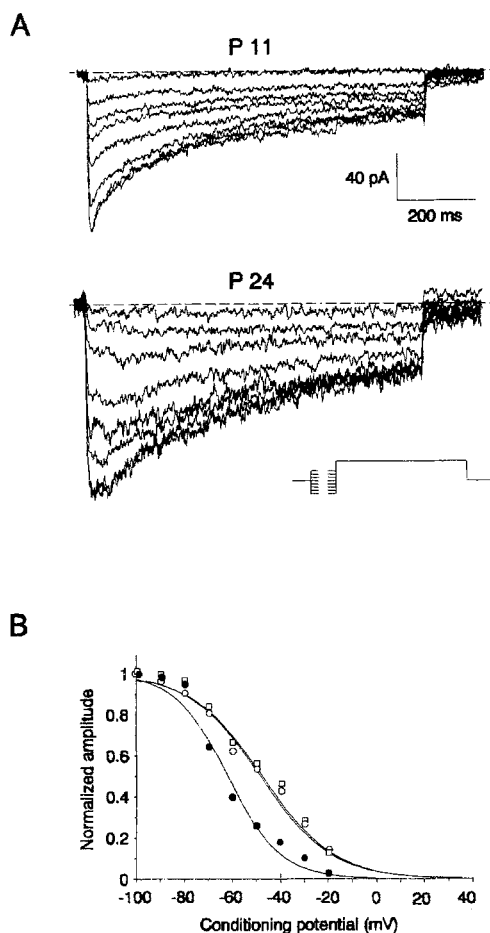
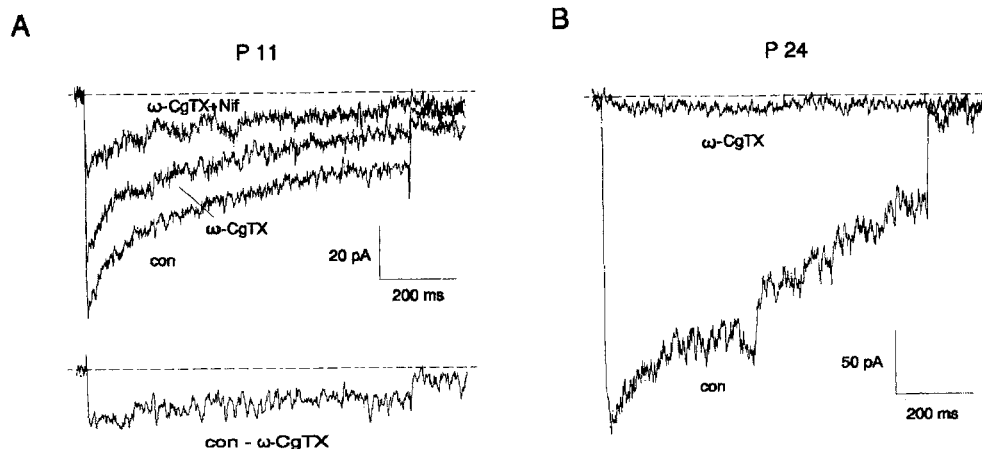


**Fig. 4A, B** Steady-state inactivation for the fast- and for the slow-inactivating HVA currents component in immature ( $n=5$ , circles) and mature ( $n=5$ , squares) granule cells. **A** Two sets of current traces recorded at P11 and P24, respectively, illustrating steady-state inactivation of  $\text{Ca}^{2+}$  currents. The voltage-clamp protocol is indicated in the inset. The apparent leakage after current deactivation develops similarly as in Fig. 3A. **B** Average inactivation plots obtained with the voltage-clamp protocol illustrated in A. Data points were fit with Boltzmann equations of the form  $I/I_{\max} = 1/[1 + \exp(V - V_{1/2})/k]$  ( $R > 0.99$  for all fittings, solid lines)

**Fig. 5A, B** The effect of  $\omega$ -CgTx on HVA  $\text{Ca}^{2+}$  currents. **A** Effect of sequential application of 5  $\mu\text{M}$   $\omega$ -CgTx and 5  $\mu\text{M}$  nifedipine at P11. The lower trace is obtained by digital subtraction of the  $\omega$ -CgTx-sensitive component from control. **B** Effect of 5  $\mu\text{M}$   $\omega$ -CgTx application at P24. These currents were obtained as indicated in Fig. 3A (holding potential = -60 mV, conditioning potential = -100 mV, test potential = 0 mV). The apparent leakage after current deactivation develops similarly as in Fig. 3A



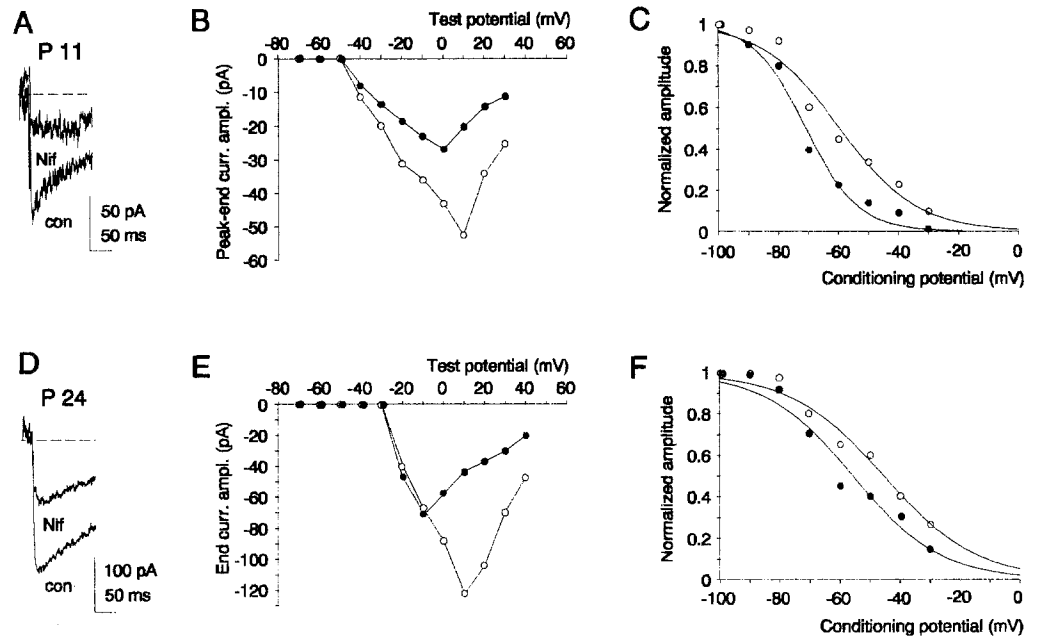
The dihydropyridine nifedipine is considered to be a selective blocker of L-type HVA currents. Nifedipine reduced HVA currents both in immature and mature preparations. In immature preparations (Fig. 6A) application of 5  $\mu\text{M}$  nifedipine reduced the fast-inactivating current component ( $49 \pm 9\%$ ,  $n=5$ ) and the slow inactivating component as well ( $46 \pm 7\%$ ,  $n=5$ ). Also in mature preparations (Fig. 6D) nifedipine reduced the slow-inactivating component ( $41 \pm 5\%$ ,  $n=6$ ). Therefore, nifedipine exerted a similar percentage of block on both the fast- and slow-inactivating components. Nifedipine action on the slow-inactivating component overlapped with that of  $\omega$ -CgTx, as clearly shown by a comparison of Figs. 5B and 6D, and by the percentages of block. The action of nifedipine on the fast-inactivating component was not affected by the previous action of  $\omega$ -CgTx on the persistent component (Fig. 5A). Nifedipine block was partially reversed by washing.

To investigate the mechanism of nifedipine action, we constructed  $I/V$  (Fig. 6B, E) and steady-state inactivation plots (Fig. 6C, F) for the fast- and slow-inactivating components. Nifedipine shifted the peak of the  $I/V$  relationships and the inactivation curves by about 10 mV towards more negative potentials (fast-inactivating component:  $V_{1/2} = -60$  mV,  $k=13$  in control, vs  $V_{1/2} = -71$  mV,  $k=9$  after nifedipine; slow-inactivating component:  $V_{1/2} = -45$  mV,  $k=16$  in control, vs  $V_{1/2} = -56$  mV,  $k=15$  after nifedipine). Similar results obtained from cardiac cells were interpreted in terms of modification of channel gating operated by the  $\text{Ca}^{2+}$  antagonist [22].

Application of 5  $\mu\text{M}$  Bay K 8644, a dihydropyridine with mixed agonist/antagonist action, caused a small reduction both of the fast-inactivating current component in immature granule cells ( $14 \pm 4\%$ ,  $n=6$ ) and of the slow-inactivating component at all ages ( $16 \pm 5\%$ ,  $n=11$ ). Reduction of the HVA current by Bay K 8644 had already been reported in different neurons [5].

$\text{Ni}^{2+}$  (40  $\mu\text{M}$ ) reduced the fast-inactivating current component by  $34 \pm 16\%$  ( $n=6$ ) in immature granule cells, matching the value obtained by Ellinor et al. [16] at the same concentration in cerebellar granule cells in culture. However, the slow-inactivating component (measured both in mature and immature HVA currents) was almost

**Fig. 6A–F** The effect of nifedipine on HVA  $\text{Ca}^{2+}$  currents. **A, D** Current traces before and after 5  $\mu\text{M}$  nifedipine at P11 and P24, respectively. **B, C** Average *I/V* and inactivation plots for the fast-inactivating component in immature currents ( $n=5$ ). Data were obtained before (*open circles*) and after (*filled circles*) 5  $\mu\text{M}$  nifedipine application. Inactivation plots were fit with Boltzmann equations ( $R>0.99$ ). **E, F** Average *I/V* and inactivation plots for the persistent component in mature granule cells ( $n=6$ ). Data were obtained before (*open circles*) and after (*filled circles*) 5  $\mu\text{M}$  nifedipine application. Inactivation plots were fitted with Boltzmann equations ( $R>0.99$ ). In *I/V* plots SEM averaged 24% of the mean data values, in inactivation plots SEM averaged 13% of the mean



insensitive to  $\text{Ni}^{2+}$  ( $4\pm 5\%$ ,  $n=3$ ).  $\text{Cd}^{2+}$  (40–500  $\mu\text{M}$ ) also blocked the HVA current at all ages. The block by either  $\text{Ni}^{2+}$  or  $\text{Cd}^{2+}$  was reversed by reperfusion with control saline.

Sensitivity to the funnel web spider Agelenopsis aperta toxin (FTX) was reported in immature dissociated granule cells [3]. Application of 200 nM of the purified fraction  $\omega$ -Aga-IVA [26] caused a small reduction of the fast-inactivating ( $10\pm 8\%$ ,  $n=9$ ) and slow-inactivating component ( $16\pm 6\%$ ,  $n=9$ ) in immature granule cells.

## Discussion

$\text{Ca}^{2+}$  currents recorded from cerebellar granule cells in situ showed different kinetics, gating, and pharmacology at different stages of development. Our results suggest that the changes of  $\text{Ca}^{2+}$  currents can be explained as the coexistence of HVA currents with distinguishable features, which are expressed in different proportions during development.

A fast-inactivating current component predominated in immature granule cells and then disappeared after maturation. A slow-inactivating current component, very small at early stages of development, progressively increased during maturation, and remained the only sizeable component after maturation. The global effect consisted of an increase and slowing down of the  $\text{Ca}^{2+}$  current.

In several types of neurons inactivation of HVA current is  $\text{Ca}^{2+}$  dependent [19]. In granule cells two lines of evidence indicate that inactivation of the fast-inactivating current is not  $\text{Ca}^{2+}$  dependent: first,  $\text{Ba}^{2+}$  and  $\text{Ca}^{2+}$  currents have similar kinetics; second, steady-state inactivation occurs in a voltage range where  $\text{Ca}^{2+}$  currents are

not activated. Independence of a fast-inactivating component of HVA currents from  $\text{Ca}^{2+}$  was previously reported in cerebellar granule cells in culture [31].

Neuronal maturation is often characterized by increased structural complexity. However, no remarkable increase of the dendritic and axonal arborization, nor of the soma surface extension, occurs in cerebellar granule cells at the ages considered here [1, 20]. Accordingly,  $C_m$ , which is proportional to the area of the clamped membrane surface, did not change remarkably, and the voltage-clamp rate was similar in mature as in immature neurons (see also [12, 13]). Since  $\tau_{vc}$  was around 110  $\mu\text{s}$ , the voltage-clamp was tens to hundreds of times faster than  $\text{Ca}^{2+}$  currents. Considering that estimated voltage- and space-clamp errors are negligible ( $<2.3\%$ ), evidence reported above supports the conclusion that the different kinetics observed were not the effect of changed electrotonic properties during granule cell maturation. Consistently,  $\text{Ca}^{2+}$  currents deactivated with time constants shorter than 1 ms, and did not show kinetic distortions attributable to inappropriate voltage-clamp. We also recall that parallel fibres were severed in parasagittal slices, minimizing the potential contribution of  $\text{Ca}^{2+}$  currents originating at remote presynaptic sites which may escape from somatic voltage-clamp. Indeed, granule cells expressing fast- and slow-inactivating  $\text{Ca}^{2+}$  current components similar to those reported in our experiment were recorded from granule cells in culture [31]. In those experiments, however, no correlation with development could be established.

## HVA current properties

The fast-inactivating current activates and inactivates at potentials more negative than the slow-inactivating cur-

rent. Moreover, the fast-inactivating current is faster to activate and to inactivate, and its kinetics are less voltage dependent than those of the slow-inactivating current. Since current decay was 2 orders of magnitude slower than rising phase, coupling of activation with inactivation might contribute to slow down the rising phase of mature HVA currents at negative membrane potentials.

Fast- and slow-inactivating HVA currents display clear differential sensitivity to  $\omega$ -CgTx. The fast-inactivating current is almost insensitive to  $\omega$ -CgTx which, by contrast, reduces strongly the slow-inactivating current (94% in mature and 60% in immature preparations). The action of nifedipine, on the other hand, is similar on both currents (49% and 41% of block on fast- and slow-inactivating currents respectively). Therefore, the data obtained with  $\omega$ -CgTx and nifedipine indicate L-type pharmacological properties for the fast-inactivating current and both L- and N-type pharmacological properties for the slow-inactivating current.

In some respects, according to its biophysical properties, blockade by  $\text{Ni}^{2+}$  and insensitivity to Bay K 8644, the fast-inactivating current bears a striking resemblance to the current studied by Ellinor et al. [16] in granule cells in culture. That current, however, was insensitive to dihydropyridine block. Nifedipine presumably acted by modifying  $\text{Ca}^{2+}$  channel gating in our experiments, as originally reported in cardiac muscle cells [22]. It may be that control of gating by dihydropyridines requires a factor(s) which was not effective in culture. It cannot be excluded, however, that in spite of their similarity, our fast-inactivating component and Ellinor's current [16] are generated by different channels. The rather negative activation of the fast-inactivating component resembles also a property of P-channel currents [24]. However, since there is no clear blocking action of the selective toxin  $\omega$ -Aga-IVA, the fast inactivating component is probably not mediated by P-channels.

Comparison of average percentages of block of the slow-inactivating current measured in two different groups of cells suggests a certain degree of overlap between the actions of  $\omega$ -CgTx and nifedipine. Similar to ours, mixed pharmacology has been observed already by De Waard et al. [14] comparing nicardipine and  $\omega$ -CgTx action in cerebellar granule cells in culture, while in other neurons in culture no overlap was observed [27]. It should be noted that the overlap was not demonstrated when comparing nifedipine and  $\omega$ -CgTx action in the same cell, so that overlap may be the apparent result of a variable extent of block in different cells. The nature of overlap, therefore remains unclear.

The present results suggest that the different properties of granule cell HVA  $\text{Ca}^{2+}$  currents reported previously [14, 16, 25, 31] may be in the large part explained in terms of different stages of granule cell development in culture. Our data do not provide evidence, however, for the presence of P-channel currents reported in immature granule cells in culture [3].

One or multiple channels for the two components?

The coexistence of multiple HVA  $\text{Ca}^{2+}$  currents is not a specific property of cerebellar granule cells, since it has been reported already in isolated hippocampal [36] and neocortical neurons [18]. The molecular nature of this multiplicity is, however, still unclear. In cultured granule cells, single-channel recordings supported the view that biphasic HVA currents were generated by access to two inactivation states of the same channel [31, 32]. This model fits with our observation that nifedipine blocked to a similar extent both the fast- and slow-inactivating current components. This model, however, is in contrast with the rather selective sensitivity of the slow-inactivating but not of the fast-inactivating component to  $\omega$ -CgTx, which suggests the existence of two distinct populations of  $\text{Ca}^{2+}$  channels. Channel multiplicity may also occur within the slow-inactivating component itself, which may result from the contribution of at least two channel populations showing similar kinetic and gating properties, but different pharmacological properties. Indeed, different gating patterns and pharmacological properties were recognized in  $\text{Ca}^{2+}$  channel currents recorded from membrane patches of cerebellar granule cells in culture [6, 17], suggesting that more than one type of  $\text{Ca}^{2+}$  channel is expressed.

The mechanism generating the shift from the immature to the mature form of the  $\text{Ca}^{2+}$  channel remains speculative. Expression of new  $\alpha$ -subunits, association of the  $\alpha$ -subunit with different regulatory  $\beta$ -subunits [16], endogenous modulation [28, 29], and compartmentalization and "trapping" of  $\text{Ca}^{2+}$  channels in specific neuronal regions [34] may be involved. At present, we have no conclusive means to distinguish between these possibilities. Single-channel recording from granule cells in cerebellar slices would probably be needed to answer these questions.

#### Biological aspects of $\text{Ca}^{2+}$ current development

The absolute increase of the HVA  $\text{Ca}^{2+}$  current was due to increased density of  $\text{Ca}^{2+}$  channels, as observed also during growth of cerebellar granule cells [25] and dorsal root ganglion (DRG) sensory neurons, in culture [4].  $\text{Ca}^{2+}$  current density reached  $0.06 \text{ mA/cm}^2$  after maturation, comparable to values reported in other neurons [8, 10].

The time course of  $\text{Ca}^{2+}$  current maturation (see Fig. 2) was similar to that of the  $\text{Na}^{2+}$  current [13], and to that of synaptic non-NMDA receptors in the same age-window [12]. The observation of spontaneous synaptic activity only in those granule cells which showed sizeable  $\text{Ca}^{2+}$  currents, suggests a strict time relationship between  $\text{Ca}^{2+}$  current maturation and mossy fibre synapse formation and development [13, 20], although no causal relationship between synapse formation and  $\text{Ca}^{2+}$  current maturation has been demonstrated so far. The amplitude of  $\text{Ca}^{2+}$  currents, as well as that of  $\text{Na}^{2+}$  currents and non-NMDA receptor currents, attains

plateau at P20, in coincidence with the end of the major phase of granule cell maturation [1, 20, 30]. It is tempting to conclude that the  $\text{Ca}^{2+}$  current properties observed at more than P20 are representative of adult granule cells, although further changes can still occur at later stages.

HVA currents increased in PC12 cells under the influence of nerve growth factor (NGF) [34], and in neuroblastoma cells stimulated with differentiating agents [10, 37]. Moreover, NGF reduced HVA current inactivation [34] and increased the fraction of current blocked irreversibly by  $\omega$ -CgTx [29]. Therefore, although the factors stimulating the expression and differentiation of  $\text{Ca}^{2+}$  currents in granule cells are unknown so far, it is worth noting that changes of the HVA current were similar to those induced by trophic agents in cell cultures.

It should be noted that in five immature cells we also observed a  $\text{Ca}^{2+}$  current with LVA properties associated with the HVA current (not shown). In these cells the current transient elicited by hyperpolarizing voltage pulses was comparatively slower and  $C_m$  greater ( $C_m=13\pm 2.8$  pF,  $n=5$ ) than that usually observed in granule cells, which suggests that these cells were Golgi cells.

## Conclusions

The action of specific  $\text{Ca}^{2+}$  channel blockers suggests a greater complexity at the molecular level than the simple distinction that can be achieved between a fast- and a slow-inactivating HVA current [24, 35]. Nonetheless, the biophysical distinction of the two components is relevant to the possible roles played by  $\text{Ca}^{2+}$  channels during maturation. In the immature neuron, cytoplasmic  $\text{Ca}^{2+}$  build-up would activate already with small depolarizations and then cease within 50–100 ms. In the mature neuron,  $\text{Ca}^{2+}$  entry would follow stronger depolarizations, and then last longer due to reduced time- and voltage-dependent inactivation. These properties may play a role in determining different excitable properties of cerebellar granule cells at different developmental stages [E. D'Angelo, G. De Filippi and P. Rossi, unpublished observation].

**Acknowledgements** We would like to thank Drs. T. Knoepfel and S. M. Thompson for their comments on the manuscript. This work was supported by grants of the "Ministero della Ricerca Scientifica e Tecnologica" and "Consorzio Interuniversitario Nazionale di Fisica della Materia". Dr. P. Rossi was supported by a grant of Crinos S.p.A., Villa Guardia (Como).

## References

- Altman J (1982) Morphological development of the rat cerebellum and a source of its mechanism. In: Chan-Palay V, Palay S (eds) *The cerebellum: new vistas*. Springer, Berlin Heidelberg New York, pp 8–49
- Bertolino M, Llinas RR (1992) The central role of voltage-activated and receptor-operated calcium channels in neuronal cells. *Annu Rev Pharmacol Toxicol* 32:399–421
- Bertolino M, Vicini S, Llinas RR, Costa E (1990) Voltage-dependent calcium currents in rat cerebellar granule neurons (CGN). *Soc Neurosci Abstr* 16:956
- Bickmeyer U, Muller E, Wiegand H (1993) Development of calcium currents in cultures of mouse spinal cord and dorsal root ganglion neurones. *Neuroreport* 4:131–134
- Boll W, Lux HD (1986) Blockade of neuronal calcium conductances by organic antagonists. *Exp Brain Res* 14:104–111
- Bossu JL, De Waard M, Fagni L, Tanzi F, Feltz A (1994) Characteristics of Ca channels responsible for voltage-activated Ca entry in rat cerebellar granule cells. *Eur J Neurosci* 6:335–344
- Burgoyne RD, Cambray-Deakin MA (1988) The cellular neurobiology of neuronal development: the cerebellar granule cell. *Brain Res Rev* 13:77–101
- Carbone E, Lux HD (1987) Kinetics and selectivity of a low-voltage-activated calcium current in chick and rat sensory neurones. *J Physiol (Lond)* 386:547–570
- Carbone E, Swandulla D (1989) Neuronal calcium channels: kinetics, blockade and modulation. *Prog Biophys Mol Biol* 54:31–58
- Carbone E, Sher E, Clementi F (1990) Ca currents in human neuroblastoma IMR32 cells: kinetics, permeability and pharmacology. *Pflügers Arch* 416:170–179
- D'Angelo E, Rossi P, Garthwaite J (1990) Dual-component NMDA receptor currents at a single central synapse. *Nature* 346:467–470
- D'Angelo E, Rossi P, Taglietti V (1993) Different proportions of N-methyl-D-aspartate and non-N-methyl-D-aspartate receptor currents at the mossy fibre-granule cell synapse of developing rat cerebellum. *Neuroscience* 53:121–130
- D'Angelo E, Rossi P, De Filippi G, Magistretti J, Taglietti V (1994) The relationship between synaptogenesis and development of voltage-dependent currents in cerebellar granule cells in situ. *J Physiol (Paris)* 88:197–207
- De Waard M, Feltz A, Bossu JL (1991) Properties of a high-threshold voltage-activated calcium current in rat cerebellar granule cells. *Eur J Neurosci* 3:771–777
- Edwards FA, Konnerth A, Sakmann B, Takahashi T (1989) A thin slice preparation for patch-clamp recordings from neurons of the mammalian central nervous system. *Pflügers Arch* 414:600–612
- Ellinor PT, Zhang J-F, Randall AD, Zhou M, Schwarz TL, Tsien RW, Horne WA (1993) Functional expression of a rapidly inactivating neuronal calcium channel. *Nature* 363:455–458
- Forti L, Pietrobon L (1993) Functional diversity of L-type calcium channels in rat cerebellar neurons. *Neuron* 10:437–450
- Giffin K, Solomon JS, Burkhalter A, Nerbonne JM (1991) Differential expression of voltage-gated calcium channels in identified visual cortical neurons. *Neuron* 6:321–332
- Gutnick MJ, Lux HD, Swandulla D, Zucker H (1989) Voltage-dependent and calcium dependent inactivation of calcium channel current in identified snail neurones. *J Physiol (Lond)* 412:197–220
- Hamori J, Somogyi J (1983) Differentiation of cerebellar mossy fiber synapses in the rat: a quantitative electron microscope study. *J Comp Neurol* 220:365–377
- Haws CM, Slesinger PA, Lansman JB (1993) Dihydropyridine- and w-conotoxin-sensitive  $\text{Ca}^{2+}$  currents in cerebellar neurons: persistent block of L-type channels by a pertussis toxin-sensitive G-protein. *J Neurosci* 13:1148–1156
- Hess P, Lansman JB, Tsien RW (1984) Different modes of Ca channel gating behavior favoured by dihydropyridine Ca agonists and antagonists. *Nature* 311:538–544
- Komuro H, Rakic P (1992) Selective role of N-type calcium channels in neuronal migration. *Science* 257:806–809
- Llinas R, Sugimori M, Hillman DE, Cherksey B (1992) Distribution and functional significance of the P-type voltage-dependent  $\text{Ca}^{2+}$  channels in the mammalian central nervous system. *Trends Neurosci* 15:351–355
- Marchetti C, Carignani C, Robello M (1991) Voltage-dependent calcium currents in dissociated granule cells from cat cerebellum. *Neuroscience* 43:121–133

26. Mintz IM, Venema VJ, Swiderek KM, Lee TD, Bean BP, Adams ME (1992) P-type calcium channels blocked by the spider toxin  $\omega$ -Aga-IVA. *Nature* 355:827–829
27. Minth IM, Adams ME, Bean BP (1993) P-type calcium channels in rat central and peripheral neurons. *Neuron* 9:85–95
28. Plummer MR, Hess P (1991) Reversible uncoupling of inactivation in N-type calcium channels. *Nature* 351:657–659
29. Plummer MR, Logothetis DE, Hess P (1989) Elementary properties and pharmacological sensitivities of calcium channels in mammalian peripheral neurons. *Neuron* 2:1453–1463
30. Puro DG, Woodward DJ (1977) Maturation of evoked mossy fibre input to rat cerebellar Purkinje cells. *Exp Brain Res* 28:427–441
31. Slesinger PA, Lansman JB (1991) Inactivation of calcium currents in granule cells cultured from mouse cerebellum. *J Physiol (Lond)* 435:101–121
32. Slesinger PA, Lansman JB (1991) Inactivating and non-inactivating dihydropyridine-sensitive  $\text{Ca}^{2+}$  channels in mouse cerebellar granule cells. *J Physiol (Lond)* 439:301–323
33. Spruston N, Jaffe DB, Williams SH, Johnston D (1993) Voltage- and space-clamp errors associated with measurement of electrotonically remote synaptic events. *J Neurophysiol* 70:781–802
34. Streit J, Lux HD (1990) Calcium current inactivation during nerve-growth-factor-induced differentiation of PC12 cells. *Pflügers Arch* 416:368–374
35. Swandulla D, Carbone E, Lux HD (1991) Do calcium channel classifications account for neuronal calcium channel diversity? *Trends Neurosci* 14:46–51
36. Thompson SM, Wong RKS (1991) Development of calcium current subtypes in isolated rat hippocampal pyramidal cells. *J Physiol (Lond)* 439:671–689
37. Toselli M, Masetto S, Rossi P, Taglietti V (1991) Characterization of a voltage-dependent calcium current in the human neuroblastoma cell line SH-SY5Y during differentiation. *Eur J Neurosci* 3:514–522
38. Traynelis SF, Silver RA, Cull-Candy SG (1993) Estimated conductance of glutamate receptor channels activated during EPSCs at the cerebellar mossy fiber-granule cell synapse. *Neuron* 11:279–289
39. Yaari Y, Hamon B, Lux HD (1987) Development of two types of calcium channels in cultured mammalian hippocampal neurons. *Science* 235:680–682